# Direct observation of tin sites and their reversible interconversion in zeolites by solid-state NMR spectroscopy

Guodong Qi[1], Qiang Wang[1], Jun Xu[1], Qinming Wu[2], Chao Wang[1], Xingling Zhao[1], Xiangju Meng[2], Fengshou Xiao[2] & Feng Deng[1]

Metal-substituted zeolites are an important type of solid Lewis acid with a wide range of applications. Despite the importance of this type of catalyst, identifying active sites can be challenging because different types of metal sites experience similar environments in zeolites. Here we show direct observation of different tin sites in Sn-β zeolite. Two types of open tin sites are unambiguously identified via correlating the hydroxyl groups to Sn atoms with one- and two-dimensional proton-detected $^1$H/$^{119}$Sn correlation solid-state NMR spectroscopy, which only amounts to ca. 17% of the total tin content. A reversible transformation between the open and closed tin site is observed. The results provide valuable insights into the nature of tin sites in Sn-β zeolite and open an avenue for the use of proton-detected solid-state NMR methods for characterization of metal sites in zeolite catalysts.

[1] National Centre for Magnetic Resonance in Wuhan, State Key Laboratory of Magnetic Resonance and Atomic and Molecular Physics, Key Laboratory of Magnetic Resonance in Biological Systems, Wuhan Institute of Physics and Mathematics, Chinese Academy of Sciences, Wuhan 430071, China. [2] Department of Chemistry, Zhejiang University, Hangzhou 310028, China. These authors contributed equally: Guodong Qi, Qiang Wang. Correspondence and requests for materials should be addressed to J.X. (email: xujun@wipm.ac.cn) or to F.D. (email: dengf@wipm.ac.cn)

Zeolites are among the most important heterogeneous catalysts in the modern chemical and petrochemical industries. Metals are often introduced into zeolites to alter their acidity and thus their catalytic activity. The formation of Lewis acid sites by metals such as tin, titanium, and zirconium in zeolites leads to distinct activities in many important industrial reactions[1–7]. Tin-substituted Sn-β zeolite represents a breakthrough in the exploitation of atom-efficient solid Lewis acid catalyst for green and sustainable production of chemicals and fuels[2] because of its unparalleled catalytic performance in transformation of biomass and biomass-derived feedstocks[7–16] such as isomerization of glucose[8,9] and conversion of sugars to lactic acid[7] and furan derivatives[11] as well as in the important reactions of Baeyer−Villiger oxidations[2] and Meerwein−Ponndor−Verley reduction[3]. Due to the great potential of the Sn-β zeolite for upgrading renewable energy sources, considerable efforts have been devoted to the synthesis and characterization of Sn-β zeolites[17–22].

Hydrothermal[2] and postsynthetic[19–23] strategies have been developed to introduce Sn into β zeolite. It is generally accepted that isomorphously substituted Sn (IV) sites are responsible for the high activity of Sn-β zeolite[14,24]. However, the similar coordination environment of different Sn sites results in great difficulties in their spectroscopic discrimination. Different techniques have been attempted for the detection of Sn sites in Sn-β[17–19]. Infrared (IR) spectroscopy of probe molecules in combination with theoretical calculations suggests the formation of so-called open (e.g., $(SiO)_3Sn–OH$) and closed (e.g., $(SiO)_4Sn$) Sn sites on hydrothermally synthesized Sn-β[25,26]. For the open site, the defect-open and hydrolyzed-open configurations were further proposed[27], both of them contain the Sn–OH moieties, although the open structure with outer-sphere coordination of $SiO^-$ and coordinately unsaturated Sn forming frustrated Lewis pair was also hypothesized to be present on Sn-β[28]. Solid-state NMR is a powerful tool for the characterization of the active site in zeolites. However, the low concentration of Sn loading (usually lower than 2 wt%) and low isotope abundance of NMR active $^{119}Sn$ nucleus (8.6%) is an obstacle for NMR detection and reasonable analysis of the obtained signals in low signal-to-noise ratio. Nevertheless, octahedral and tetrahedral Sn sites were differentiated based on the chemical shift of $^{119}Sn$ on the hydrated and dehydrated Sn-β with isotopically enriched $^{119}Sn$ atoms[2,12,29,30]. In order to enhance the detecting sensitivity, the dynamic nuclear polarization surface-enhanced NMR spectroscopy (DNP-SENS) technique[27,31–33] was recently applied on Sn-β zeolites. With the help of DFT calculations, hydrated closed and open Sn sites were proposed in postsynthetic Sn-β[32], while the Sn species was claimed to exist mainly in closed state in Sn-β zeolite synthesized by the direct hydrothermal method[27]. Since water molecules or additional solvent and radicals used for DNP experiments could be adsorbed on the two types of Sn sites acting as the proton sources to enhance the $^{119}Sn$ signal[27,31–33], the Sn sites with and without associated hydroxyl group were unable to be discriminated from $^{119}Sn$ NMR signal alone. In addition, probably due to its low content and interference from the large quantity of silanols of zeolite, the open site with Sn–OH group in Sn-β is difficult to be directly identified by $^1H$ NMR or IR.

With respective to activity of the Sn sites, the hydroxyl group associated open one was proved to be the active site in the reactions such as Baeyer–Villiger oxidation of cyclohexanone[25] and glucose isomerization[26,34,35]. Additionally, the high activity of the open site was also theoretically suggested by DFT calculations based on cluster models[36]. However, by far, no experimental technique is available to unambiguously identify the active open Sn site. Besides, the relationship between the open and closed Sn states still remains elusive. Rational design of Sn-containing zeolites with higher activity and selectivity can only be achieved by fully understanding the structure and nature of their active sites.

Here we show that proton-detected $^1H/^{119}Sn$ double-resonance correlation solid-state NMR spectroscopy can be used to unambiguously characterize the Sn active sites in Sn-β zeolites. Two types of open Sn sites containing Sn–OH groups are directly identified by one-dimensional (1D) and two-dimensional (2D) $^1H\{^{119}Sn\}$ dipolar-mediated (D-) HMQC NMR spectroscopy at high field and fast MAS speed, which only amounts to ca. 17% of the total Sn sites. In combination with 2D $^1H\{^{29}Si\}$ D-HMQC NMR experiment, a reversible transformation between the open and closed Sn sites is ascertained.

## Results

**Probing tin sites and Sn–OH groups.** A Sn-β zeolite containing 1.2 wt.% of Sn was prepared by the direct hydrothermal method[2,37] (denoted as Sn-β). In order to enhance NMR sensitivity, an isotope $^{119}Sn$ ($^{119}Sn$, 97.4%)-enriched Sn-β zeolite was synthesized and denoted as $^{119}Sn$-β. For comparison, a pure silica β zeolite was also synthesized and denoted as Si-β. Scanning electron microscopy-energy dispersive spectrometer (TEM-EDS), X-ray powder diffraction (XRD), $^{29}Si$ MAS NMR and diffuse reflectance ultraviolet-visible (DR-UV-vis) analyses showed that all the obtained samples were well crystallized with the topological structure of zeolite β and the metal Sn atoms were homogeneously incorporated into the framework of zeolite β (Supplementary Figs 1–4). $^{119}Sn$ MAS NMR experiments were performed to study the coordination states of framework Sn sites on $^{119}Sn$-β. As shown in Supplementary Fig. 5, there are three 6-coordinated framework Sn sites, and they can be transformed into 4-coordinated Sn sites after dehydration at a temperature above 393 K. Either closed or open Sn sites could contribute to the observed $^{119}Sn$ signals from the 4-coordinated Sn atoms in the framework of β zeolite[27]. No signal is visible in the $^1H$-$^{119}Sn$ CP MAS NMR spectrum of the dehydrated $^{119}Sn$-β even with 80 h of acquisition (Supplementary Fig. 5 c and d). This is due to the dramatically reduced cross-polarization efficiency from $^1H$ to $^{119}Sn$ spins caused by the absence of adsorbed water. The open Sn site featured by the bound hydroxyl group cannot be readily detected by the $^1H$-$^{119}Sn$ CP MAS NMR, most likely because of its low concentration.

Owing to the high sensitivity of $^1H$ nuclei, $^1H$ MAS NMR experiments at high field (18.8 T) were conducted on the $^{119}Sn$-β zeolites (Fig. 1a–e). In order to probe the spatial proximity/interaction between $^1H$ and $^{119}Sn$ atoms, 1D proton-detected[38,39] $^1H\{^{119}Sn\}$ D-HMQC MAS NMR experiments were also carried out at a MAS speed of 40 kHz (Fig. 1f–k). Indeed, we also tried to perform J-HMQC experiments[40,41]; however, the small J-couplings and fast relaxations in the zeolites hinder their practical implementation on our samples. As shown in Fig. 1a, a main signal at 4.1 ppm and three weak $^1H$ signals at 0.8, 1.2 and 5.4 ppm are observable in hydrated $^{119}Sn$-β. The signals at 0.8 and 1.2 ppm come from a trace of residual template, which was confirmed by comparing with those of uncalcined $^{119}Sn$-β. After the sample being dehydrated at room temperature (Fig. 1b), the 4.1 ppm signal shifts to high field (3.9 ppm) and is attenuated remarkably, while there is no obvious change on the 5.4 ppm signal, indicating that the two signals probably belong to two types of adsorbed water molecules. Note that only the signal at 5.4 ppm remains in the 1D $^1H\{^{119}Sn\}$ D-HMQC MAS NMR spectrum (Fig. 1f, h) in which only the protons interacting with Sn species can be observable, suggesting that this $^1H$ signal is associated with water molecules chemically adsorbed on Sn sites. In contrast, the strong signals at 4.1 and 3.9 ppm are completely suppressed, indicative of the absence of Sn atoms in close proximity. Thus, we can assign these two signals to physically adsorbed water molecules in zeolite channels. When the
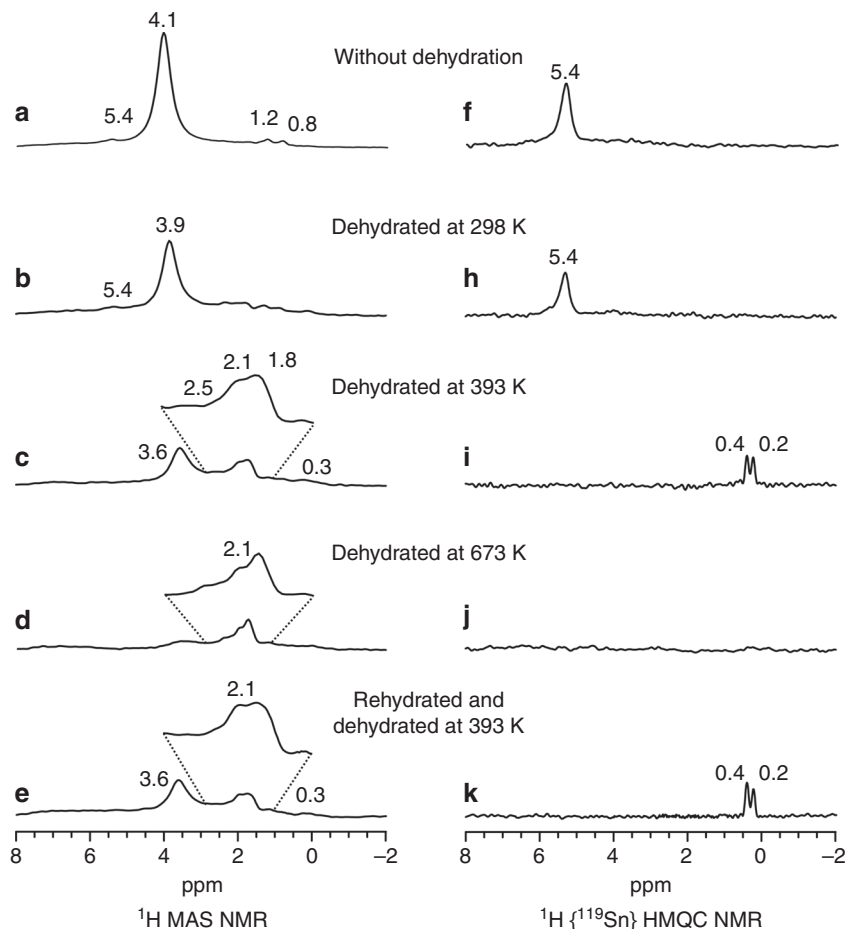
**Fig. 1** Solid-state proton NMR of open Sn sites in Sn-β zeolite. $^1$H MAS NMR spectra (**a-e**) and $^1$H {$^{119}$Sn} D-HMQC MAS NMR spectra (**f-k**) of $^{119}$Sn-β with different dehydration and rehydration treatments

dehydration temperature is increased to 393 K, new signals appear at 2.5, 2.1, and 1.8 ppm in the $^1$H MAS NMR spectrum (Fig. 1c). The three signals can be assigned to different kinds of non-hydrogen-bonded Si–OH species while a broad signal at 3.6 ppm may come from hydrogen-bonded SiOH groups[42,43]. They disappeared in the corresponding HMQC spectrum (Fig. 1i). Indeed, the formation of Si–OH species is confirmed by $^1$H-$^{29}$Si CP MAS NMR experiments (Supplementary Fig. 3). It is interesting to note that a weak broad signal at 0.3 ppm is visible in the $^1$H MAS NMR spectrum (Fig. 1c), which produces two well-resolved peaks at ~0.4 and ~0.2 ppm in the corresponding 1D $^1$H {$^{119}$Sn} HMQC spectrum (Fig. 1i). Considering the $^1$H-$^{119}$Sn CP NMR result together, the observation allows us to conclude that two Sn–OH groups are probably present on the dehydrated $^{119}$Sn-β. When $^{119}$Sn-β zeolite was dehydrated at 673 K, the two Sn–OH signals at 0.4 and 0.2 ppm completely disappear in the 1D $^1$H{$^{119}$Sn} HMQC spectrum (Fig. 1j), which is accompanied by a slight decline of the Si–OH signal at 2.1 ppm in the $^1$H MAS NMR spectrum (Fig. 1d) as compared with that at 393 K (Fig. 1c). After the 673 K dehydrated sample was rehydrated (exposed in air moisture for 30 days) and then dehydrated at 393 K, the two signals at 0.2 and 0.4 ppm appear again (Fig. 1k) accompanied with the recovery of the Si–OH signal at 2.1 ppm (Fig. 1e). This indicates a reversible formation of Sn–OH groups in Sn-β. Note that Sn–OH species is unobservable in the 1D $^1$H {$^{119}$Sn} HMQC spectra when the chemically adsorbed water (5.4 ppm) is not removed (Fig. 1f, h). Since such water molecules are most likely adsorbed on framework Sn atoms forming 6-coordinated Sn sites, we suspect that the relatively

large amount of water molecules and the low concentration of Sn–OH species make the Sn–OH undetectable.

**Connectivity between tin atoms and hydroxyl groups**. To get insight into the local structure of Sn sites in $^{119}$Sn-β, 2D $^1$H {$^{119}$Sn} D-HMQC spectra were recorded (see Fig. 2). The spectra with full chemical shift range of $^1$H and $^{119}$Sn are shown in Supplementary Fig. 6. Both hydrated $^{119}$Sn-β and the corresponding sample dehydrated at 298 K exhibit a similar $^1$H–$^{119}$Sn correlation peak at (5.4, −686) ppm (Fig. 2a, b), revealing the presence of water molecule-bound 6-coordinated Sn sites. This is also in agreement with the $^1$H-$^{119}$Sn CP MAS NMR result that the $^{119}$Sn signal at −686 ppm is selectivity enhanced by the neighboring protons from chemically adsorbed water molecules (Supplementary Fig. 5a). For $^{119}$Sn-Beta dehydrated at 393 K, four $^1$H-$^{119}$Sn correlation peaks are observable in the HMQC spectrum (Fig. 2c). The two 4-coordinated Sn sites at −443 and −429 ppm are correlated to $^1$H species at 0.1–0.4 ppm. Further analysis shows that the two $^1$H signals at 0.37 and 0.20 ppm have correlations with the Sn signal at −443 ppm while the two $^1$H signals at 0.34 and 0.17 ppm exhibit correlations with the Sn signal at −429 ppm (Fig. 2c). It is interesting to note that when $^{119}$Sn decoupling was applied during $^1$H acquisition in the D-HMQC experiments, the four correlation peaks merge into two ones centered at (0.28, −443) and (0.26, −429) ppm (Fig. 2d). Therefore, the four resolved correlation peaks in Fig. 2c should be due to the doublet splitting of two types of $^1$H signals caused by J-coupling between spin pairs of $^1$H and $^{119}$Sn. We further measured
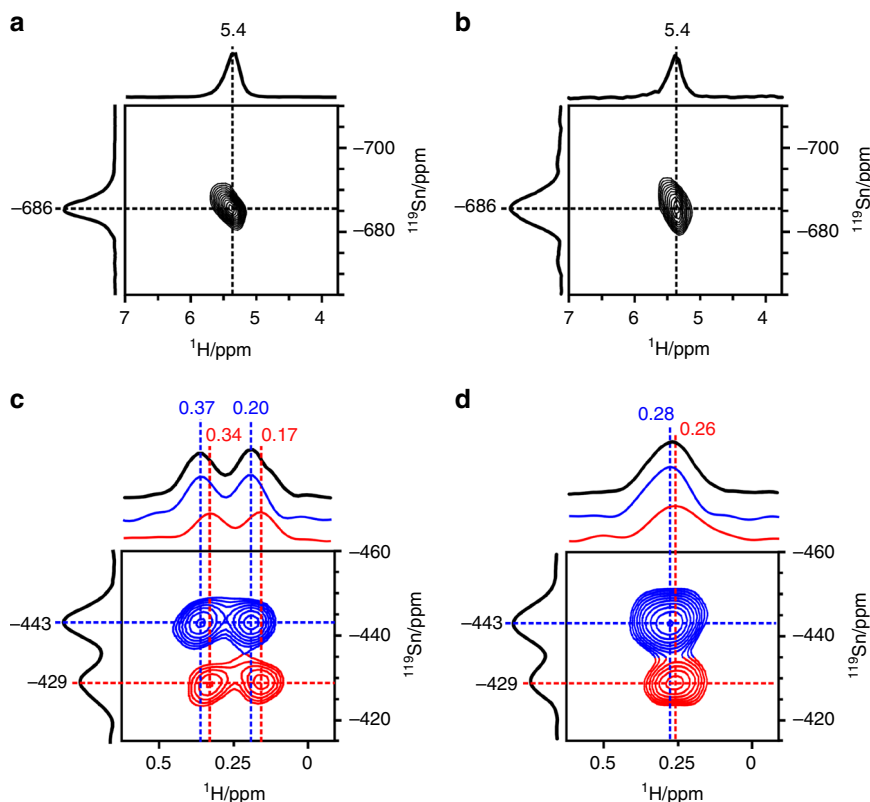
**Fig. 2** Identification of open Sn sites by proton-detected $^1H/^{119}Sn$ correlation NMR. Two-dimensional $^1H\{^{119}Sn\}$ HMQC MAS NMR spectra of $^{119}Sn$-β **a** without dehydration, **b** dehydrated at 298 K, **c** dehydrated at 393 K without $^{119}Sn$ decoupling, and **d** dehydrated at 393 K with $^{119}Sn$ decoupling. Projections of $^1H$ and $^{119}Sn$ dimensions are shown in black. Representative slices along −429 ppm (red) and −443 ppm (blue) in the F1 dimension are also displayed in **c** and **d**

the $J$-coupling constant from the peak distance between the doublet fine structure, which was determined to be ~136 Hz, in consistent with the $^2J$ ($^{119}Sn$–$^1H$) constant of 130 Hz for Sn–OH species in monoalkyl-SnCl$_{3-x}$(OH)$_x$ solution[44,45]. These results provide strong evidence that there are two types of Sn–OH groups; one corresponds to the Sn atom at −443 ppm bound to the hydroxyl group at 0.28 ppm, and the other is the Sn atom at −429 ppm bound to the hydroxyl group at 0.26 ppm. They can be attributed to two types of open Sn sites ((SiO)$_3$Sn–OH) located at different T sites on the framework of β zeolite. This is in agreement with the recent DFT study, which indicated that there are two T sites to stabilize the open Sn sites on β zeolite[46]. Here the two types of open Sn sites were directly observed under dehydration condition without addition of solvent and radicals, and the influences of water, solvent, and radicals can be excluded. To the best of our knowledge, this is the first time to unambiguously identify two types of open Sn sites on Sn-β zeolite, which shows different NMR characteristics in the proton-detected $^1H\{^{119}Sn\}$ double-resonance correlation spectra. The direct observation of the Sn–OH groups indicates that either defect- or hydrolyzed-open sites are present, although they are formed differently on the sample[27].

On the basis of $^1H\{^{119}Sn\}$ D-HMQC NMR results, the $^{119}Sn$ MAS NMR spectra of samples dehydrated at 393 and 673 K were deconvoluted (Fig. 3): the signals at −443 and −429 ppm correspond to the open sites and the signals at −446, −441 and −422 ppm come from the closed Sn sites. Accordingly, the content of two types of Sn sites could be estimated. As listed in Table 1, the open Sn sites is ca. 17% of the total Sn sites on the sample dehydrated at 393 K, in consistent with that (ca. 20%) previously determined by site titration with IR adsorption of CD$_3$CN[25]. Higher temperature dehydration (673 K) leads to the
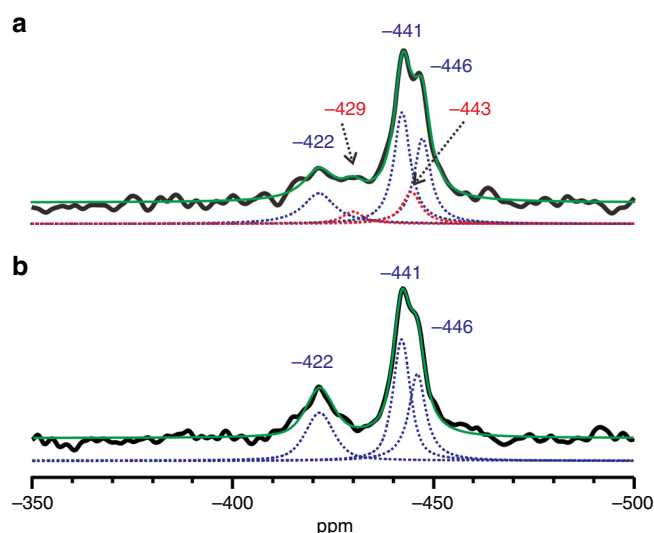


**Fig. 3** Quantitative $^{119}Sn$ solid-state NMR analysis of Sn sites in Sn-β. Deconvolution of $^{119}Sn$ MAS NMR spectra of $^{119}Sn$-β zeolites dehydrated at 393 K (**a**) and 673 K (**b**). Solid lines show experimental (black) and simulated (green) spectra, and dash lines show the individual components of closed (blue) and open (red) Sn sites

drop of the open sites to zero with the generation of closed sites due to the dehydroxylation of the Sn–OH groups[47].

**Interconversion of open and closed tin sites.** The transformation of the open site into the closed one could be responsible for

the disappearance of NMR signals of Sn–OH groups in the 1D [1]H {[119]Sn} D-HMQC MAS spectrum (Fig. 1j) during the dehydration process. In order to gain more insight into this process, 2D ^{1}H {^{29}Si} D-HMQC NMR experiments were performed on [119]Sn-Beta with different degrees of dehydration (Fig. 4). For the sample dehydrated at 393 K (Fig. 4a), the appearance of correlation peaks between ^{1}H signals at 1.8, 2.1, 2.5, and 3.6 ppm and [29]Si signal at −102 ppm indicates the presence of different types of Si–OH groups (Q$_3$ sites, Si(OSi)$_3$OH). It is noteworthy that the correlation peak of Q$_3$ site at (2.1, −102) ppm is evidently reduced when the sample is dehydrated at 673 K (Fig. 4b), indicating its low stability in the dehydroxylation process. This is also confirmed by comparing the Q$_3$ sites on the representative slices along ^{1}H signals at 1.8, 2.1, and 2.5 ppm (Supplementary Fig. 7). These Q$_3$

sites could be involved in dehydration with (SiO)$_3$Sn–OH species, leading to the transformation of open Sn site to closed one ((SiO)$_4$Sn). When the sample is rehydrated, the closed Sn site could be hydrolyzed to regenerate an open Sn site which is visible after the sample is dehydrated at 393 K (Fig. 1k).

Taking all the results together, the Sn active sites and their evolutions observed on Sn-β zeolite can be pictured (Fig. 5). Both closed and open Sn sites are present and there is a reversible conversion between them. The defect-open or hydrolyzed-open sites are not differntiated here. In hydrated sample, two water molecules are chemically adsorbed on the same Sn atom, forming a 6-coordinated open Sn site (Fig. 5a). After the removal of the chemically adsorbed water molecules by dehydration at 393 K, a 4-coordinated open Sn site is isolated (Fig. 5b). Further increasing the dehydration temperature to 673 K causes the removal of water between the 4-coordinated open Sn site and the neighboring Si–OH group, leading to the formation of a 4-coordinated closed Sn site (Fig. 5c). This is responsible for the disappearance of the open Sn site and the only presence of the closed one on the highly dehydrated Sn-β. However, the closed Sn site shows reactivity to water molecules even at room temperature. The Sn–O–Si bond of the closed Sn site can be broken by the attack of water molecules, through which the closed Sn site is reversely transformed into an open one by forming the Sn–OH group[47]. Note that the recovery of open Sn site from closed one is a slow process (in air moisture for 30 days) at room temperature. We found that a quick saturation adsorption of water (in 24 h) onto the [119]Sn-β zeolite dehydrated at

**Table 1 Content of closed and open Sn sites on Sn-β zeolites dehydrated at 393 and 673 K**

| Sn sites | 393 K[a] | 673 K[a] |
|---|---|---|
| Closed (−446 ppm) | 28 (0.34) | 33 (0.40) |
| Closed (−441 ppm) | 36 (0.43) | 41 (0.49) |
| Closed (−422 ppm) | 19 (0.23) | 26 (0.31) |
| Open (−443 ppm) | 12 (0.14) | 0 (0) |
| Open (−429 ppm) | 5 (0.06) | 0 (0) |

[a] The percentages normalized to total Sn sites are listed while the amount of Sn sites in wt.% estimated by multiplying the total Sn content (1.2 wt.%) are listed in parentheses
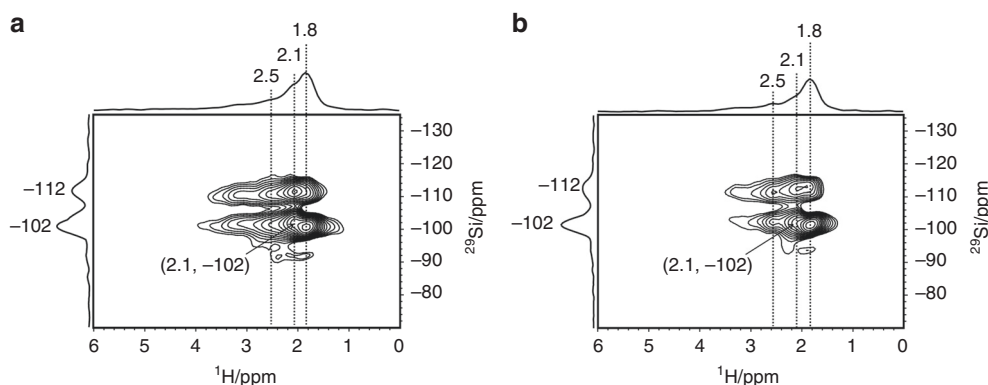


**Fig. 4** Proton-detected ^{1}H/^{29}Si correlation NMR. ^{1}H {^{29}Si} D-HMQC MAS NMR spectra of [119]Sn-β dehydrated at (**a**) 393 K and (**b**) 673 K
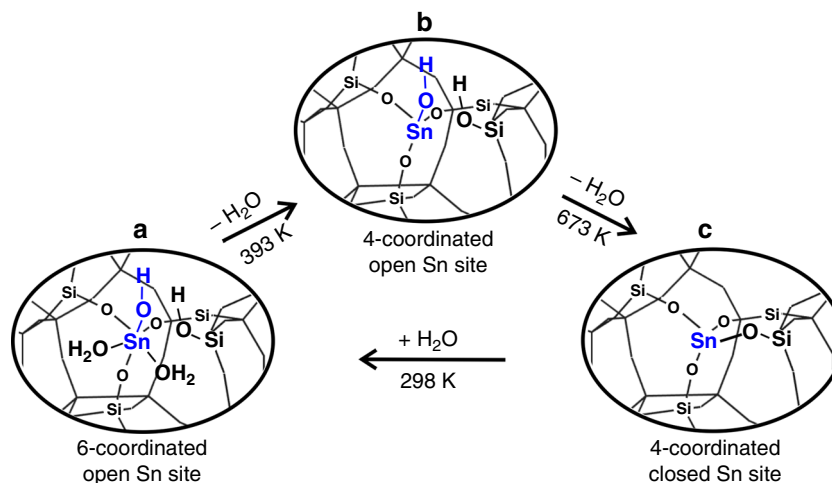


**Fig. 5** Proposed model for interconversion between open and closed Sn sites in Sn-β zeolite. **a** 6-coordinated open Sn site, **b** 4-coordinated open Sn site, and **c** 4-coordinated closed Sn site

673 K in a Petri dish did not lead to the generation of open Sn sites (Supplementary Fig. 8). Instead, a moderate heating of the hydrated sample at 393 K in air facilitates their formation.

## Discussion

In summary, open Sn sites containing Sn–OH groups in Sn-β are unambiguously identified and quantified. 2D $^1H$ {$^{119}Sn$} D-HMQC MAS NMR spectroscopy enables differentiation of two types of open Sn sites by correlating the hydroxyl groups and associated Sn species. Both open and closed Sn sites are present and the transformation between them is reversible on Sn-β zeolite. This information provides valuable insights into the nature of active Sn sites in Sn-β zeolite. Hydroxyl groups containing metal species in zeolites such as TS-1 are often thought to be the active sites[48–50], which however are hardly identified due to the low concentration and similar environment to coexisting metal sites. Our results have important implications for the characterization of active metal sites in zeolites in particular for those with different metal speciation, which is essential for fine-tuning and rational design of catalysts.

## Methods

**Sample preparation**. Sn-β zeolites were synthesized by direct hydrothermal method in fluoride medium[2]. Typically, 8.5 g of tetraethyl orthosilicate (TEOS; Sinopharm Chemical Reagent Co., Ltd, 99%) was hydrolyzed in 12.7 g aqueous solution of 25% tetraethylammonium hydroxide (TEAOH; J&K Scientific) under stirring. Then a solution containing 0.09 g $SnCl_4 \cdot 5H_2O$ (Sinopharm Chemical Reagent Co., Ltd, 99%) was added, and the mixture was stirred until the ethanol formed upon hydrolysis of TEOS was evaporated. About 1.2 mL 40% HF (Sinopharm Chemical Reagent Co., Ltd, 98%) was added to the obtained clear solution (ca. 12 g), and a thick paste was formed. Then, an aqueous suspension of 0.10 g Si-β seeds was added. For Si-β seeds, commercial Al-β was treated with 70% nitric acid (Sinopharm Chemical Reagent Co., Ltd, 98%) followed by filtration and drying, and then the dealuminated Si-β was obtained as seeds. The mixture containing Si-β seeds was evaporated in the fume hood, resulting in a final gel with the composition (mole ratio) of: 1.0 $SiO_2$:0.0062 Sn:0.55 TEAOH:7.5 $H_2O$:0.55 HF. Then, the ca. 10.50 g of mixture was transferred into an 18 mL Teflon-lined stainless-steel autoclave was placed in a preheated oven and kept at 413 K for 30 days in static state. Finally, the solid product was recovered by filtration and washing. Typically, 1.00 g sample was washed by 100 mL deionized water for more than three times, until the $Cl^-$ ions was completely removed. The sample was then dried at 353 K overnight followed by calcination at 873 K for 10 h. For calcination, 0.30 g sample was placed in a 1.5 cm × 4.0 cm quartz boat and calcined at static state air condition with a temperature program of 3 K/min to 873 K, then holding 10 h at 873 K. The isotope $^{119}Sn$-enriched $^{119}Sn$-β zeolite was prepared by a similar route, using a solution of $^{119}Sn$ precursor[37], which was prepared by dissolving of 0.03 g $^{119}Sn$ metal foil (ISOFLEX, USA, $^{119}Sn$ abundance 97.4%) into 0.2 mL aqueous solution with an appropriate amount of 37% hydrochloric acid (Sinopharm Chemical Reagent Co., Ltd, 98%) and 30 % hydrogen peroxide (Sinopharm Chemical Reagent Co., Ltd, 98%) at 323 K. After the hydrochloric acid solution was evaporated at 393 K, the obtained white solid was dissolved into 1 mL water. The Si-β zeolite was synthesized with Si-β seeds by the hydrothermal method in fluoride media without adding any Sn precursor.

Calcined $^{119}Sn$-β zeolites were dehydrated at 298, 393, and 673 K with a pressure of $10^{-3}$ Pa on a vacuum line over a period of 2 h.

**SEM-EDS experiments**. SEM-EDS experiments were performed on a Hitachi FE-SEM SU8010 field-emission scanning electron microscope; the accelerating voltage was operated at 5 kV.

**DR-UV-vis experiments**. DR-UV-vis spectra were collected on an Agilent Cary 4000 UV-Vis spectrometer at room temperature. The scan rate is 2 nm/s for DR-UV-vis measurements.

**XRD experiments**. XRD patterns were recorded on a Panalytical X' Pert PRO X-ray diffractometer (40 kV, 40 mA) using CuKα ($\lambda = 1.5406$ Å) radiation. The scan rate is 0.05° per second for XRD measurements.

**Solid-state NMR experiments**. $^{29}Si$ MAS NMR and $^1H$-$^{29}Si$ CP MAS NMR experiments were carried out at 7.05 T on a Varian Infinity plus-300 spectrometer with a 7.5 mm double-resonance probe. The resonance frequencies were 299.78 and 59.55 MHz for $^1H$ and $^{29}Si$, respectively. Single-pulse $^{29}Si$ MAS experiments with $^1H$ decoupling were performed by using a $\pi/2$ pulse width of 6.2 μs and a repetition time of 60 s. $^1H$-$^{29}Si$ CP MAS experiments were performed by using a contact time of 4 ms and with a repetition time of 2 s. The magic angle spinning

rate was set to 4 kHz. The $^{29}Si$ chemical shift was referenced to kaoline at −91.0 ppm, as the second reference to tetramethylsilane.

$^{119}Sn$ MAS NMR and $^1H$-$^{119}Sn$ CP MAS NMR experiments were carried out at 7.05 T on a Varian Infinity plus-300 spectrometer with a 4 mm double-resonance probe. The resonance frequencies were 299.78 MHz and 111.72 MHz for $^1H$ and $^{119}Sn$, respectively. Single-pulse excitation $^{119}Sn$ MAS experiments were performed on the zeolite samples by using a $\pi/2$ pulse width of 4.6 μs, a repetition time of 200 s, and a magic angle spinning rate of 12 kHz. $^1H$-$^{119}Sn$ CP MAS experiments were performed by using a contact time of 4 ms and a repetition time of 20 s. The $^{119}Sn$ chemical shift was referenced to tetracyclohexyltin at −97.4 ppm. Each spectrum was accumulated for ca. 80 h.

$^1H$ MAS, $^1H$ {$^{119}Sn$} D-HQMC and $^1H$ {$^{29}Si$} D-HQMC NMR experiments were carried out at 18.8 T on a Bruker Avance$^{III}$ 800 spectrometer, using a 1.9 mm HX double-resonance probe at a spinning rate of 40 kHz. The resonance frequencies were 800.36, 298.33, and 158.99 MHz for $^1H$, $^{119}Sn$, and $^{29}Si$, respectively. $^1H$ MAS NMR experiments were performed on the zeolite samples by using the Hahn-echo pulse sequence ($\pi/2 - \tau - \pi - \tau$ –acquisition) with a $\pi/2$ pulse width of 2.0 μs and a repetition time of 20 s, where $\tau$ equals to three rotor period (75 μs).

The pulse sequence for $^1H$ {$^{119}Sn$/$^{29}Si$} D-HMQC experiments is illustrated in Supplementary Fig. 9. The rf field strength for the $^1H$ $\pi/2$ and $\pi$ pulses was set to 125 kHz. The pulse lengths for $\pi/2$ pulses on the $^{119}Sn$ channel or $^{29}Si$ channel were fixed to 3.3 or 3.7 μs, respectively. SR4 recoupling on the $^1H$ channel was used with $\nu_{nut1H}$ = 80 kHz, the total recoupling time $\tau$ was set to 1200 and 2000 μs for $^1H$ {$^{119}Sn$} and $^1H$ {$^{29}Si$} D-HMQC experiments, respectively. The fast MAS and short recoupling time makeit possible to mainly detect the correlations corresponding to the stronger interactions between $^1H$ and $^{119}Sn$ atoms in 2D $^1H$ {$^{119}Sn$} D-HMQC experiments. The low-power continuous-wave $^{119}Sn$ decoupling, with an amplitude of ~3 kHz, was used during the $^1H$ acquisition in the Fig. 2d and Supplementary Fig. 6d. Except for these two spectra, no decoupling was applied during the acquisition of the 2D D-HMQC spectra. The increment interval in the indirect dimension was set to 25 μs. Typically, 2D $^1H$ {$^{119}Sn$} D-HMQC spectra were acquired using 30 increments and 320 scans, and 2D $^1H$ {$^{29}Si$} D-HMQC spectra were acquired using 40 increments and 240 scans. The recycle delay was set to 8 s.

## References

1. Huybrechts, D. R. C., Debruycker, L. & Jacobs, P. A. Oxyfunctionalization of alkanes with hydrogen peroxide on titanium silicate. *Nature* **345**, 240–242 (1990).

2. Corma, A., Nemeth, L. T., Renz, M. & Valencia, S. Sn-zeolite beta as a heterogeneous chemoselective catalyst for Baeyer-Villiger oxidations. *Nature* **412**, 423–425 (2001).

3. Corma, A., Domine, M. E., Nemeth, L. & Valencia, S. Al-free Sn-beta zeolite as a catalyst for the selective reduction of carbonyl compounds (Meerwein −Ponndorf−Verley reaction). *J. Am. Chem. Soc.* **124**, 3194–3195 (2002).

4. Sushkevich, V. L., Ivanova, I. I., Tolborg, S. & Taarning, E. Meerwein-Ponndorf-Verley-Oppenauer reaction of crotonaldehyde with ethanol over Zr-containing catalysts. *J. Catal.* **316**, 121–129 (2014).

5. Van de Vyver, S. & Román-Leshkov, Y. Metalloenzyme-like zeolites as Lewis acid catalysts for C-C bond formation. *Angew. Chem. Int. Ed.* **54**, 12554–12561 (2015).

6. Palagin, D., Sushkevich, V. L., Ivanova, I. I. & Coupling, C.-C. Catalyzed by zeolites: is enolization the only possible pathway for aldol condensation? *J. Phys. Chem. C* **120**, 23566–23575 (2016).

7. Holm, M. S., Saravanamurugan, S. & Taarning, E. Conversion of sugars to lactic acid derivatives using heterogeneous zeotype catalysts. *Science* **328**, 602–605 (2010).

8. Moliner, M., Román-Leshkov, Y. & Davis, M. E. Tin-containing zeolites are highly active catalysts for the isomerization of glucose in water. *Proc. Natl. Acad. Sci. USA* **107**, 6164–6168 (2010).

9. Román-Leshkov, Y., Moliner, M., Labinger, J. A. & Davis, M. E. Mechanism of glucose isomerization using a solid Lewis acid catalyst in water. *Angew. Chem. Int. Ed.* **49**, 8954–8957 (2010).

10. Taarning, E. et al. Zeolite-catalyzed biomass conversion to fuels and chemicals. *Energy Environ. Sci.* **4**, 793–804 (2011).

11. Nikolla, E., Román-Leshkov, Y., Moliner, M. & Davis, M. E. "One-Pot" synthesis of 5-(hydroxymethyl)furfural from carbohydrates using tin-beta zeolite. *ACS Catal.* **1**, 408–410 (2011).

12. Bermejo-Deval, R. et al. Metalloenzyme-like catalyzed isomerizations of sugars by Lewis acid zeolites. *Proc. Natl. Acad. Sci. USA* **109**, 9727–9732 (2012).

13. Kubicka, D., Kubickova, I. & Cejka, J. Application of molecular sieves in transformations of biomass and biomass-derived feedstocks. *Catal. Rev.* **55**, 1–78 (2013).

14. Dapsens, P. Y., Mondelli, C. & Perez-Ramirez, J. Design of Lewis-acid centres in zeolitic matrices for the conversion of renewables. *Chem. Soc. Rev.* **44**, 7025–7043 (2015).

15. Ennaert, T. et al. Potential and challenges of zeolite chemistry in the catalytic conversion of biomass. *Chem. Soc. Rev.* **45**, 584–611 (2016).

16. Luo, H. Y., Lewis, J. D. & Román-Leshkov, Y. Lewis acid zeolites for biomass conversion: perspectives and challenges on reactivity, synthesis, and stability. *Annu. Rev. Chem. Biomol. Eng.* **7**, 663–692 (2016).

17. Bare, S. R. et al. Uniform catalytic site in Sn-beta-zeolite determined using X-ray absorption fine structure. *J. Am. Chem. Soc.* **127**, 12924–12932 (2005).

18. Roy, S., Bakhmutsky, K., Mahmoud, E., Lobo, R. F. & Gorte, R. J. Probing Lewis acid sites in Sn-beta zeolite. *ACS Catal.* **3**, 573–580 (2013).

19. Tang, B. et al. Improved postsynthesis strategy to Sn-beta zeolites as Lewis acid catalysts for the ring-opening hydration of epoxides. *ACS Catal.* **4**, 2801–2810 (2014).

20. Li, P. et al. Postsynthesis and selective oxidation properties of nanosized Sn-beta zeolite. *J. Phys. Chem. C* **115**, 3663–3670 (2011).

21. Hammond, C., Conrad, S. & Hermans, I. Simple and scalable preparation of highly active Lewis acidic Sn-beta. *Angew. Chem. Int. Ed.* **51**, 11736–11739 (2012).

22. Dijkmans, J. et al. Post-synthesis Snβ: an exploration of synthesis parameters and catalysis. *J. Catal.* **330**, 545–557 (2015).

23. Vega-Vila, J. C., Harris, J. W. & Gounder, R. Controlled insertion of tin atoms into zeolite framework vacancies and consequences for glucose isomerization catalysis. *J. Catal.* **344**, 108–120 (2016).

24. Corma, A. & Garcia, H. Lewis acids as catalysts in oxidation reactions: from homogeneous to heterogeneous systems. *Chem. Rev.* **102**, 3837–3892 (2002).

25. Boronat, M., Concepcion, P., Corma, A., Renz, M. & Valencia, S. Determination of the catalytically active oxidation Lewis acid sites in Sn-beta zeolites, and their optimisation by the combination of theoretical and experimental studies. *J. Catal.* **234**, 111–118 (2005).

26. Harris, J. W. et al. Titration and quantification of open and closed Lewis acid sites in Sn-Beta zeolites that catalyze glucose isomerization. *J. Catal.* **335**, 141–154 (2016).

27. Wolf, P. et al. Correlating synthetic methods, morphology, atomic-level structure, and catalytic activity of Sn-β catalysts. *ACS Catal.* **6**, 4047–4063 (2016).

28. Dijkmans, J. et al. An inner-/outer-sphere stabilized Sn active site in β-zeolite: spectroscopic evidence and kinetic consequences. *ACS Catal.* **6**, 31–46 (2016).

29. Dijkmans, J. et al. Cooperative catalysis for multistep biomass conversion with Sn/Al beta zeolite. *ACS Catal.* **5**, 928–940 (2015).

30. Bermejo-Deval, R., Gounder, R. & Davis, M. E. Framework and extraframework tin sites in zeolite beta react glucose differently. *ACS Catal.* **2**, 2705–2713 (2012).

31. Gunther, W. R., Michaelis, V. K., Caporini, M. A., Griffin, R. G. & Román-Leshkov, Y. Dynamic nuclear polarization NMR enables the analysis of Sn-beta zeolite prepared with natural abundance [119]Sn precursors. *J. Am. Chem. Soc.* **136**, 6219–6222 (2014).

32. Wolf, P. et al. NMR signatures of the active sites in Sn-beta zeolite. *Angew. Chem. Int. Ed.* **53**, 10179–10183 (2014).

33. Wolf, P. et al. Identifying Sn site heterogeneities prevalent among Sn-beta zeolites. *Helv. Chim. Acta* **99**, 916–927 (2016).

34. Bermejo-Deval, R., Orazov, M., Gounder, R., Hwang, S. J. & Davis, M. E. Active sites in Sn-beta for glucose isomerization to fructose and epimerization to mannose. *ACS Catal.* **4**, 2288–2297 (2014).

35. Hwang, S.-J. et al. Solid state NMR characterization of Sn-beta zeolites that catalyze glucose isomerization and epimerization. *Top. Catal.* **58**, 435–440 (2015).

36. Yang, G., Pidko, E. A. & Hensen, E. J. M. The mechanism of glucose isomerization to fructose over Sn-BEA zeolite: a periodic density functional theory study. *Chemsuschem* **6**, 1688–1696 (2013).

37. Kolyagin, Y. G., Yakimov, A. V., Tolborg, S., Vennestrøm, P. N. R. & Ivanova, I. I. Application of ^{119}Sn CPMG MAS NMR for fast characterization of Sn sites in zeolites with natural [119]Sn isotope abundance. *J. Phys. Chem. Lett.* **7**, 1249–1253 (2016).

38. Wiench, J. W., Bronnimann, C. E., Lin, V. S. Y. & Pruski, M. Chemical shift correlation NMR spectroscopy with indirect detection in fast rotating solids: studies of organically functionalized mesoporous silicas. *J. Am. Chem. Soc.* **129**, 12076–12077 (2007).

39. Palmer, A. G., Cavanagh, J., Wright, P. E. & Rance, M. Sensitivity improvement in proton-detected two-dimensional heteronuclear correlation NMR spectroscopy. *J. Magn. Reson.* **93**, 151–170 (1991).

40. Lesage, A., Sakellariou, D., Steuernagel, S. & Emsley, L. Carbon−proton chemical shift correlation in solid-state NMR by through-bond multiple-quantum spectroscopy. *J. Am. Chem. Soc.* **120**, 13194–13201 (1998).

41. Wang, Q. et al. Signal enhancement of J-HMQC experiments in solid-state NMR involving half-integer quadrupolar nuclei. *Chem. Commun.* **49**, 6653–6655 (2013).

42. Freude, D., Hunger, M., Pfeifer, H. & Schwieger, W. ^{1}H MAS NMR studies on the acidity of zeolites. *Chem. Phys. Lett.* **128**, 62–66 (1986).

43. Hunger, M., Ernst, S., Steuernagel, S. & Weitkamp, J. High-field ^{1}H MAS NMR investigations of acidic and non-acidic hydroxyl groups in zeolites H-Beta, H-ZSM-5, H-ZSM-58 and H-MCM-22. *Microporous Mater.* **6**, 349–353 (1996).

44. Blunden, S. J. & Hill, R. An investigation of the base hydrolysis of methyl- and butyl-tin trichloride in aqueous solution by ^{1}H and ^{119}Sn NMR spectroscopy. *Inorg. Chim. Acta* **177**, 219–223 (1990).

45. Blunden, S. J., Smith, P. J. & Gillies, D. G. An investigation of the hydrolysis products of monoalkyltin trichlorides by [119m]Sn Mössbauer, and ^{1}H and ^{119}Sn NMR spectroscopy. *Inorg. Chim. Acta* **60**, 105–109 (1982).

46. Josephson, T. R., Jenness, G. R., Vlachos, D. G. & Caratzoulas, S. Distribution of open sites in Sn-Beta zeolite. *Microporous Mesoporous Mater.* **245**, 45–50 (2017).

47. Yakimov, A. V., Kolyagin, Y. G., Tolborg, S., Vennestrøm, P. N. R. & Ivanova, I. I. 119Sn MAS NMR study of the interaction of probe molecules with Sn-BEA: the origin of penta- and hexacoordinated tin formation. *J. Phys. Chem. C* **120**, 28083–28092 (2016).

48. Sushkevich, V. L., Palagin, D. & Ivanova, I. I. With open arms: open sites of ZrBEA zeolite facilitate selective synthesis of butadiene from ethanol. *ACS Catal.* **5**, 4833–4836 (2015).

49. Gleeson, D. et al. The architecture of catalytically active centers in titanosilicate (TS-1) and related selective-oxidation catalysts. *Phys. Chem. Chem. Phys.* **2**, 4812–4817 (2000).

50. Maschmeyer, T., Rey, F., Sankar, G. & Thomas, J. M. Heterogeneous catalysts obtained by grafting metallocene complexes onto mesoporous silica. *Nature* **378**, 159–162 (1995).

## Author contributions

G.Q., Q. Wang, C.W., and X.Z. prepared the samples and carried XRD and ^{119}Sn MAS NMR experiments. Q. Wu, X.M., and F.X. performed and analyzed the TEM-EDS and DR-UV-vis spectra. G.Q., Q. Wang, J.X., and F.D. collected and analyzed the high-field ^{1}H MAS NMR and [1]H {[119]Sn} D-HMQC spectra; G.Q., Q. Wang, J.X., and F.D. wrote the manuscript, and all authors discussed the experiments and final manuscript.

## Additional information

**Supplementary information** accompanies this paper at https://doi.org/10.1038/s42004-018-0023-1.

**Competing interests:** The authors declare no competing interests.

**Reprints and permission** information is available online at http://npg.nature.com/reprintsandpermissions/

**Publisher's note:** Springer Nature remains neutral with regard to jurisdictional claims in published maps and institutional affiliations.